



Patient-Specific Modeling of Hemodynamics: Supporting Surgical Planning in a Fontan Circulation Correction

Theodorus M. J. van Bakel¹ · Kevin D. Lau¹ · Jennifer Hirsch-Romano² · Santi Trimarchi³ · Adam L. Dorfman² · C. Alberto Figueroa^{1,4}

Received: 8 October 2017 / Accepted: 26 December 2017
© Springer Science+Business Media, LLC, part of Springer Nature 2018

Abstract

Computational fluid dynamics (CFD) is a modeling technique that enables calculation of the behavior of fluid flows in complex geometries. In cardiovascular medicine, CFD methods are being used to calculate patient-specific hemodynamics for a variety of applications, such as disease research, noninvasive diagnostics, medical device evaluation, and surgical planning. This paper provides a concise overview of the methods to perform patient-specific computational analyses using clinical data, followed by a case study where CFD-supported surgical planning is presented in a patient with Fontan circulation complicated by unilateral pulmonary arteriovenous malformations. In closing, the challenges for implementation and adoption of CFD modeling in clinical practice are discussed.

Keywords Computational fluid dynamics · Patient-specific modeling · Hemodynamics · Surgical planning · Pulmonary arteriovenous malformations · Single ventricle

Abbreviations

2D	Two-dimensional
3D	Three-dimensional
AZV	Azygos vein
CAD	Computer-aided design
CFD	Computational fluid dynamics
CT	Computed tomography
CVPA	Cavopulmonary anastomosis
FN	Fontan conduit
FSI	Fluid structure interaction

HV	Hepatic vein
HVF	Hepatic venous flow
HPC	High performance computing
IVC	Inferior vena cava
LPA	Left pulmonary artery
LINV	Left innominate vein
MRA	Magnetic resonance angiography
PAVM	Pulmonary arteriovenous malformation
PC-MRI	Phase-contrast MRI
PWV	Pulse wave velocity
RINV	Right innominate vein
RPA	Right pulmonary artery

Introduction

Hemodynamic disturbances are recognized as a triggering factor in the pathogenesis of cardiovascular disease [1]. Computational fluid dynamics (CFD) is a well-established computational technique that has been developed to study fluid flows in a variety of applications such as aerospace, automotive, and biomedical engineering. Over the past decades, numerous CFD methods have been developed to study blood flow in cardiovascular health and disease. Taylor and Figueroa wrote a comprehensive review on the methods to perform patient-specific simulations of cardiovascular mechanics [2]. To calculate hemodynamics on a patient-specific basis, CFD models can be constructed through incorporation of medical imaging and physiologic data and the use of

✉ Theodorus M. J. van Bakel
vanbakel@med.umich.edu

¹ Department of Surgery, University of Michigan, Ann Arbor, MI, USA
² University of Michigan C.S. Mott Children's Hospital Congenital Heart Center, Ann Arbor, MI, USA
³ Policlinico San Donato IRCCS, Thoracic Aortic Research Center, San Donato Milanese, Italy
⁴ Department of Biomedical Engineering, University of Michigan, Ann Arbor, MI, USA

adequate inflow and outflow boundary condition methods. These models provide high-resolution data on in vivo hemodynamics that can be used to study pathogenesis of cardiovascular diseases [3], perform noninvasive diagnostics [4], assist in medical device evaluation [5, 6], and support clinical decision making through prediction of changes in blood flow following different therapeutic interventions [7, 8].

In addition to the methodological advances noted above, faster parallel computers and user-friendly commercial software packages make patient-specific simulation of hemodynamics more accessible to clinical research settings. However, the relative user-friendliness of these tools makes it such that unqualified users can produce un-physiologic computational predictions. It is thus imperative for the user to understand key aspects of computational modeling such as mesh refinement and solution validation against clinical data.

The aim of this paper is to report on the practical aspects of using patient-specific modeling in clinical applications. First, we present a concise overview of the methods we use to construct image-based hemodynamic models in the context of clinical decision making, specifically surgical planning. Then, we present and discuss a specific case of CFD-supported surgical planning of a Fontan correction in a patient suffering from unilateral pulmonary arteriovenous malformations (PAVMs). We conclude by discussing adoption challenges for patient-specific modeling in the clinical practice and potential strategies for overcoming those challenges.

Methods for Patient-Specific Modeling of Hemodynamics

A patient-specific modeling workflow necessitates the following elements: (1) a CFD code to solve the Navier-Stokes equations, characterizing the motion of an incompressible fluid (blood) in a domain (rigid or deformable). There are numerous commercial and academic solutions, which rely either on the finite element or the finite volume methods. It is outside the scope of this work to discuss these methods in detail; (2) a three-dimensional (3D) geometric model of the vascular anatomy of interest; and (3) a set of inflow and outflow boundary conditions that represent the physiologic flow and pressure conditions of the subject. The geometric model and the inflow/outflow boundary conditions must be extracted from the available imaging and hemodynamic data (e.g., flow and pressure).

Geometric Model Construction and Mesh Generation

Vascular geometric models can be constructed from 3D imaging modalities such as computed tomography (CT) and magnetic resonance angiography (MRA) using a variety of segmentation methods. For cardiovascular applications, the

segmentation procedure seeks to delineate the boundaries of the vessels of interest in a certain region. Segmentation methods range from automatic to manual, and the outcome is either a discrete triangulated surface mesh (e.g., STereoLithography) or smooth analytical description of the vessel boundaries (e.g., computer-aided design (CAD)).

Numerous software packages offer automatic or semi-automatic methods such as threshold and region-growing algorithms that eventually produce a discrete surface triangulation. Notable examples are the open source Vascular Modeling Toolkit (www.vmtk.org) [9] and the commercial Materialise Mimics (Materialise NV, Leuven, Belgium) [10]. These methods work well on high quality image data and usually render a 3D model suitable for computational analysis within minutes. However, the resolution of the vascular model is limited by the discrete surface triangulation, and additional smoothing operations are needed in order to accommodate mesh refinement procedures.

When the image data is noisy, the segmentation process often requires significant input from the user. The custom package CRIMSON (www.cirmson.software) [11] offers semi-automatic segmentation tools whereby manually constructed centerlines and two-dimensional (2D) segmentations of the vessel lumen are used to create a CAD model of the vessels of interest via lofting operations. Analytical models offer the advantage of being easy to manipulate (e.g., adding or removing blood vessels, a critical attribute for vascular surgical planning) and because they offer a smooth surface that can easily accommodate an arbitrary number of mesh refinement operations [12]. This workflow is more time-consuming and user-dependent. The time needed to produce an analytical vascular model suitable for mesh generation depends on the size and complexity of the model. Typically, an expert user would need 60 min to create an analytical vascular model of a healthy thoracic aorta, including the supra-aortic and coronary arteries suitable for mesh generation. Creating a more complex model of, e.g., an aortic dissection would typically take 120 min, while creating a less complicated model, e.g., an abdominal aortic aneurysm, would approximately take 30 min.

Whichever workflow is chosen (analytical or surface triangulation models), a volumetric computational mesh must be created for the computational analysis. The mesh must be such that it captures not only the complex boundaries of the vascular region but also the complexities of the blood flow field. Field-mesh and mesh-adaption techniques are thus critical to ensure good quality grids that can produce mesh-independent computational results [13].

Physiologic Data and Boundary Conditions

Patient-specific hemodynamic modeling requires information on physiologic data such as cardiac output, blood pressure,

and flow splits between different vessels. Conceptually, boundary conditions on flow and/or pressure must be prescribed in all inlets and outlets of the computational model. However, in real-life clinical settings, it is nearly impossible to acquire flow and pressure data for all vessels of interest, under the same hemodynamic conditions. Therefore, numerical methods that allow the user to prescribe meaningful boundary conditions in the absence of direct measurements are critical. Multi-scale methods have been derived to couple CFD solvers for the Navier-Stokes equations with reduced-order, lumped parameter models of the circulation [14]. These models use electric-circuit analogues such as resistors, capacitors, and diodes to mimic properties such as vascular resistance, compliance, and the behavior of valves. Therefore, the reduced-order models, via the specification of meaningful values for their parameters, allow the user to include the impact of the vasculature not contained within the image data and specify boundary conditions in the absence of direct clinical measurements. The most widely used lumped parameter model is the three-element Windkessel. The parameters of these models can be obtained using either data on flow and pressure or morphometric considerations (larger vessels carry larger flows, etc.). Another strength of lumped parameter models is that they represent a convenient choice for boundary condition specification in situations in which clinical data is not directly available, such as in virtual surgical planning. Here, one can use the same pre-operatively determined lumped parameter models to represent the behavior of a distal vascular bed in the post-operative scenario (instead of a direct measurement such as a pressure or flow waveform).

Deciding which hemodynamic measurements to use for CFD modeling purposes depends primarily on the availability of the data. It is necessary to understand the acquisition methods and their limitations, as inconsistencies between data (e.g., lack of mass conservation) and measurement errors affect the simulation results [15].

Phase-contrast magnetic resonance imaging (PC-MRI) provides noninvasive data on 3D velocity maps in large blood vessels [16]. Local blood flow can then be calculated by integrating the velocity maps over the cross-sectional area of the vessel. PC-MRI velocity measurements must be acquired at each location of interest. Together with the angiography MRA sequence, the total duration of an MRI examination may range from 30 min to an hour. Consequently, changes in the physiology within the subject may occur over the examination [17]. These changes need to be identified to avoid inconsistencies in the measured data.

Duplex Doppler ultrasonography can also be used to non-invasively acquire blood flow measurements. Compared to PC-MRI techniques, Duplex Doppler ultrasonography is cheaper, faster, and more widely available in clinical practice. However, ultrasonic techniques produce operator-dependent

results, are affected by tissue signal attenuation, and thus cannot reliably be used to measure flow in deep vessels [18].

Recent developments on dynamic imaging have enabled noninvasive assessment of wall motion, producing useful information to characterize tissue strain [19, 20].

Pressure data can be obtained invasively from catheterization procedures and noninvasively from applanation tonometry or cuff measurements. Catheter measurements are the gold standard; however, they are invasive and induce hemodynamic changes through introduction of a catheter in the vessel lumen [21]. Applanation tonometry, on the other hand, can only be used for superficial vessels and is prone to measurement errors and highly operator-dependent, impacting the accuracy of the results [15]. Cuff measurements do not capture the pressure waveform over time but only the systolic and diastolic extremes at one location.

Invasive cardiac catheterization, the gold standard method to assess cardiac output, can be used to obtain simultaneous measurements of blood flow and pressure [22, 23]. The method provides direct measurements of blood pressure, and blood oxygenation, which can then be used to assess cardiac output via the Fick principle. Therefore, no information on time-resolved flow waveforms is obtained, and there is a small risk of peri-interventional complications.

Treatment of the Vessel Walls

Vessel walls are often modeled as rigid structures. This approach is computationally efficient and it produces good approximations for the velocity and pressure fields. Alternatively, the deformability of the vessels can be taken into account using fluid structure interaction (FSI) simulation techniques [24]. Here, mechanical properties such as material stiffness and vessel thickness are assigned to the vessel wall, and the elasto-dynamic equations describing wall motion are solved simultaneously with the Navier-Stokes equations. Cardiovascular FSI simulations therefore describe blood velocity and pressure, as well as wall motion, and provide a more realistic description of cardiovascular physiology, enabling calculation of quantities such as pulse wave velocity (PWV), elastic energy storage and distensibility under different hemodynamic, and/or vascular stiffness conditions [3]. FSI simulations also provide more accurate descriptions of flow quantities that are affected by the compliance of the vessel wall, such as wall shear stress. Cardiovascular FSI simulations are therefore more complex and entail significantly higher computational costs compared to those of rigid wall simulations. In practice, this means that FSI simulations take significantly more time to run, limiting their applicability in clinical practice. Furthermore, FSI simulations require time-resolved data on wall motion and wall thickness. This information is often not available in routine clinical practice. Therefore, the choice between rigid or FSI hemodynamic analysis must be made

depending on the specific quantities of interest and the availability of clinical data [25].

Computational Analysis

Once geometric model, computational mesh, and inflow and outflow boundary conditions are set, the Navier-Stokes equations are numerically solved over multiple cardiac cycles. The cardiac cycle is split in small time increments (typically in the range of $1e-3$ to $1e-4$ s) to accurately calculate blood velocity and pressure. Consequently, cardiovascular CFD simulations typically entail solving millions of equations for tens of thousands of time steps. Compared to clinical measurements, CFD simulation results have much higher spatial and temporal resolution. These analyses must therefore be run on high performance computing (HPC) systems. This is particularly important to produce solutions in clinically relevant timeframes. The time that is required to calculate the solution of a CFD simulation depends on the complexity of the model and the hardware that is being used. Typically, computations of a healthy thoracic aorta (mesh size ± 1.5 million elements), with rigid walls, take 48 h for five cardiac cycles on a HPC system with 80 cores. The same hardware would need approximately 240 h to compute solutions for a healthy thoracic aorta with deformable walls (FSI).

Computational results can be post-processed to calculate variables such as flow distribution, wall shear stress, displacement forces on medical devices [26], and metrics of hemodynamic disturbances such as turbulent kinetic energy [27] platelet activation potential [7].

Surgical Planning Supported by Computational Modeling

The current paradigm in cardiovascular surgical planning relies on anatomic assessments, results from clinical studies and the experience of the clinician performing the intervention. Different surgeons, when faced with the same problem, would often choose different surgical corrections. Furthermore, an assessment of how the hemodynamics would differ for different surgical alternatives is never made. Conceptually, this is a “trial-and-error” or “build-and-test” paradigm, which only relies on previous experiences to make choices about the current problem. In numerous engineering fields, the “build-and-test” paradigm has long been replaced by a “virtual testing” paradigm, whereby computational simulations are used to optimize the design of cars, airplanes, structures, etc. before any physical model is built.

Patient-specific computational modeling of hemodynamics therefore offers great promise to change the current paradigm in cardiovascular surgical planning. Computational modeling, if properly executed, could inform the surgeon on specific

hemodynamic differences between surgical alternatives and thus enable to theoretically identify an optimal solution based on function rather than on anatomical considerations. The optimality condition will be defined by the goals of the surgery (e.g., maximizing flow to a territory, minimizing energy losses due to turbulence, etc.). It is critically important though that the simulation workflow is set up in such a way that the computations reflect the actual anatomic and physiologic state of the patient and that the results of the predictions can be verified after the procedure is performed.

Therefore, the workflow to perform patient-specific computational simulations to support surgical planning should consist of a two-step approach. Step 1 creates a clinically validated baseline (pre-operative) solution matching anatomical and hemodynamic data. In step 2, the validated pre-operative solution is adapted to reflect different surgical options, with the goal of identifying the hemodynamically superior alternative. A schematic representation of this approach is presented in Fig. 1. In the following, we present and discuss a case of computational-supported surgical planning of a Fontan correction in a patient suffering from unilateral PAVMs.

Single Ventricle Circulation and Pulmonary Arteriovenous Malformations

A healthy cardiac configuration consists of a biventricular system supplying the pulmonary and systemic circulation. Desaturated blood from the systemic circulation enters the heart through the right atrium and gets pumped into the pulmonary circulation by the right ventricle. Blood is oxygenated in the alveoli of the lungs and returns to the left side of the heart via the pulmonary veins. From there, the oxygenated blood is pumped to the aorta to supply the systemic circulation of oxygenated blood.

Children born with an anatomic or physiologic single ventricle do not have separate systemic and pulmonary circulations in series as described above. In this configuration, oxygenated blood from the pulmonary veins is mixed with desaturated blood from the systemic veins and is ejected together into the systemic circulation. Complications resulting from this physiology are related to ventricular volume overload and hypoxia in the systemic circulation, among other problems.

To improve oxygen saturation in the systemic circulation and reduce ventricular volume overload, a Fontan circulation is surgically created in multiple stages [28]. A good overview of this surgical solution is given by Gewillig [29]. Briefly, in this circulation, the systemic venous return bypasses the heart and is directly connected to the pulmonary arteries through a cavopulmonary anastomosis (CVPA). The single ventricle is connected to the aorta and functions as the systemic pump. One important complication following CVPA is the formation of PAVMs

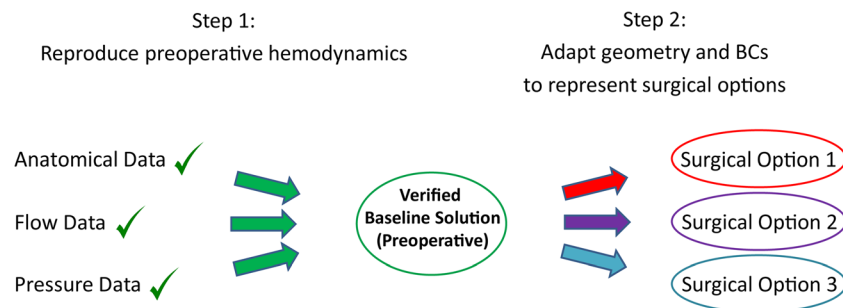


Fig. 1 Two-step workflow for image-based surgical planning: In step 1, a 3D anatomical model is constructed from the image data and boundary conditions are tuned to reproduce pre-operative hemodynamics. This step

produces a calibrated virtual representation of the hemodynamics of the patient. In step 2, the anatomical model and/or boundary conditions are adapted to reflect different surgical options. BCs = boundary conditions

[30, 31]. PAVMs are abnormal shunts between the pulmonary arteries and veins proximal to the alveoli, resulting in reduced oxygenation of blood from the affected lung returning to the heart and in elevated cardiac output due to the reduction of resistance induced by the arteriovenous shunts. Development and progression of PAVMs are attributed to the absence of hepatic venous flow (HVF), containing angiogenesis inhibitors, in the affected lung(s) [30, 31]. Revision of the Fontan circulation, aiming to direct sufficient HVF to the affected lung, has shown to reverse progression of PAVMs [32–34]. Multiple surgical options are available to reroute HVF to the lungs; however, it can be difficult to discern from traditional clinical data how the HVF is distributed over both lungs and which surgical option would result in the best hemodynamic outcome. Patient-specific computational simulations can be performed to gain detailed information on regional flow and pressure waveforms and HVF distributions to each lung. Furthermore, the impact of different surgical options on HVF distribution can be quantified to select the procedure that renders the optimal results [35].

Case Description

An 18-year-old female presented with shortness of breath and exercise intolerance at our institution. Medical history included heterotaxy syndrome with polysplenia, interrupted inferior vena cava (IVC), dextrocardia, unbalanced atrioventricular septal defect, and double outlet right ventricle with pulmonary stenosis. Surgical history included a Kawashima operation [36] at 16 months of age and insertion of an extracardiac Fontan conduit (FN) at 32 months of age. Because of the interrupted IVC, most of the systemic venous return was transported through the azygos vein (AZV). The Kawashima operation involved creation of an anastomosis between the superior vena cava, AZV, and main pulmonary artery. The base of the main pulmonary artery was ligated from the right ventricle. The FN connected the hepatic vein (HV) to the proximal left pulmonary artery to redirect HVF to the lungs, completing the Fontan circulation [29].

Clinical Data

Oxygen saturation at rest was 82%. CT imaging of the thorax revealed severe unilateral PAVMs in the right pulmonary artery (RPA). Flow measurements were acquired from PC-MRI at different locations in the Fontan circulation. Figure 2

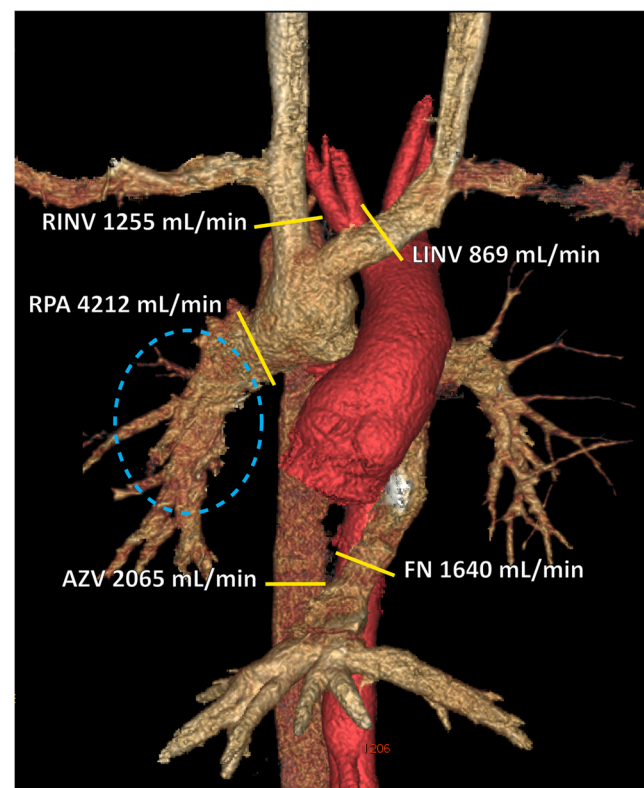


Fig. 2 CT data of the thoracic vasculature and Fontan circulation. Flow data, acquired via PC-MRI, is indicated with numerical values and yellow lines at the following locations: AZV, FN, LINV, RINV, and RPA. LPA flow could not be acquired due to artifacts induced by two embolization coils. The difference in morphology between LPA and RPA vasculatures is apparent, as a result of the pulmonary arteriovenous malformations in the RPA (circled in blue). AZV = azygos vein, CT = computed tomography, FN = Fontan conduit, LINV = left innominate vein, LPA = left pulmonary artery, PC-MRI = phase-contrast magnetic resonance imaging, RINV = right innominate vein, RPA = right pulmonary artery

presents the thoracic vascular anatomy and the measured flow data. Local pressure measurements were obtained through cardiac catheterization, as was cardiac output using the Fick principle [22].

Patient-Specific Computational Simulations

Patient-specific computational simulations were performed to gain detailed information on local distribution of HVF in the pulmonary circulation. A pre-operative 3D anatomical model was constructed from the CT imaging data using the built-in analytical segmentation tool in the validated software package CRIMSON [11]. The workflow for this procedure is presented in Fig. 3. Once the geometric model was created, boundary conditions were tuned to match the clinically measured flow and pressure data from PC-MRI and cardiac catheterization, respectively. Specifically, PC-MRI-derived flow waveforms were mapped to the FN conduit, AZV, and right and left innominate veins (RINV and LINV) using a time-varying parabolic velocity profile. The choice for parabolic velocity profiles at the inflow sections is valid for developed venous flows [37]. Three-element Windkessel models were tuned and mapped to the outlets of RPA and left pulmonary artery (LPA). An overview of the specifications of the boundary conditions at the inflow and outflow sections

is presented in Table 1. As previously mentioned, lumped parameter models are a convenient choice for outflow boundary conditions in virtual surgical planning, because they represent the behavior of the distal vascular bed (rather than a fixed flow or pressure waveform). Since we needed the simulation results within a clinically reasonable timeframe, we adopted a rigid wall assumption. We argue that alterations in the HVF distribution are mainly caused by the 3D vascular anatomy in the different surgical scenarios, rather than the vessel wall compliance. Furthermore, all scenarios are equally affected by this assumption, so this would not affect the comparison.

The patient's heart rate at time of the cardiac catheterization differed from during MRI examination. To overcome inconsistencies in the duration of the cardiac cycle, the time scale of the pressure recordings was normalized to match the time scale of the flow measurements.

Results

Baseline Simulation Results

The baseline solution successfully reproduced the patient's hemodynamics (see Fig. 4). Iterative refinements

Fig. 3 Workflow for geometric modeling using CT data in the CRIMSON software package. **a** Image data. **b** Vessel centerlines and 2D contours of the vessels of interest. **c** Lofting operations were performed and a good match between the contours of the geometric model and the image data was confirmed. **d** Completed 3D geometric CAD model. **e** The CAD model was discretized into a finite element mesh consisting of 1,768,104 linear tetrahedral elements. CAD = computed-aided design

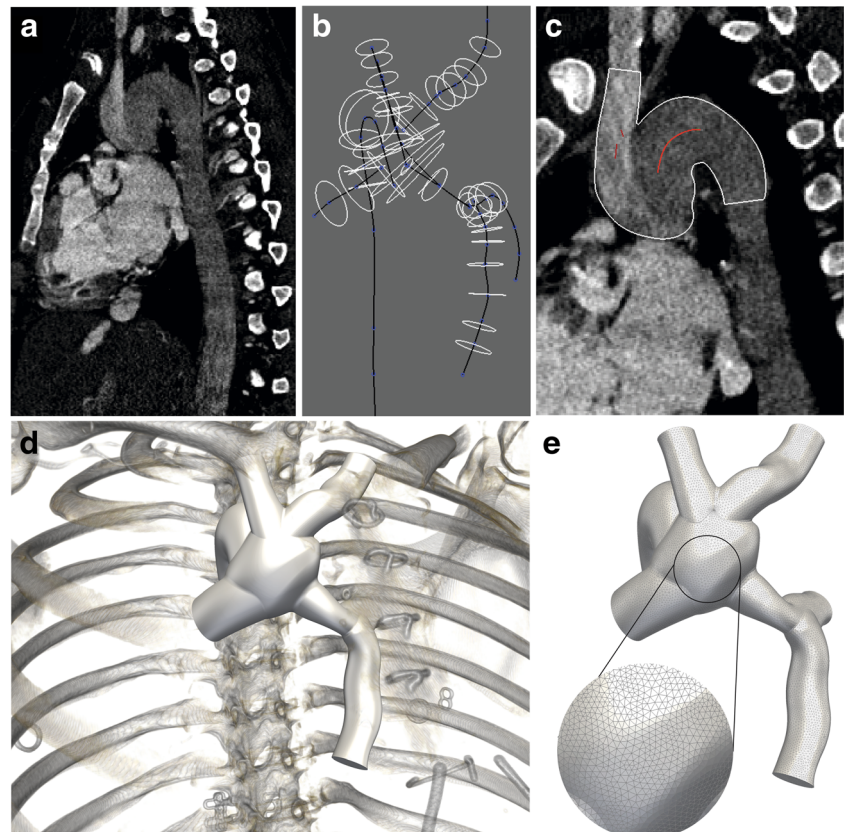


Table 1 Parameter values of boundary conditions applied at the inflow and outflow sections of the geometric model

Inflow section	Mean flow rate [mL/s]	Proportion [%]	
AZV	34.90	35.53	
FN	27.09	27.59	
LINV	14.99	15.26	
RINV	21.23	21.62	
Total	98.21	100.00	
Outflow section	Proximal resistor [Pa s/mm ³]	Capacitor [mm ³ /Pa]	Distal resistor [Pa s/mm ³]
LPA	2.64E-05	1.86E + 02	2.19E-02
RPA	5.19E-05	4.38E + 01	4.66E-02

Flow waveforms derived from phase-contrast MRI were mapped to the inflow sections, mean flow rates, and proportions of total flow are reported. On the outflow sections, three-element Windkessel models were attached and tuned to match flow and pressure measurements of the RPA and LPA

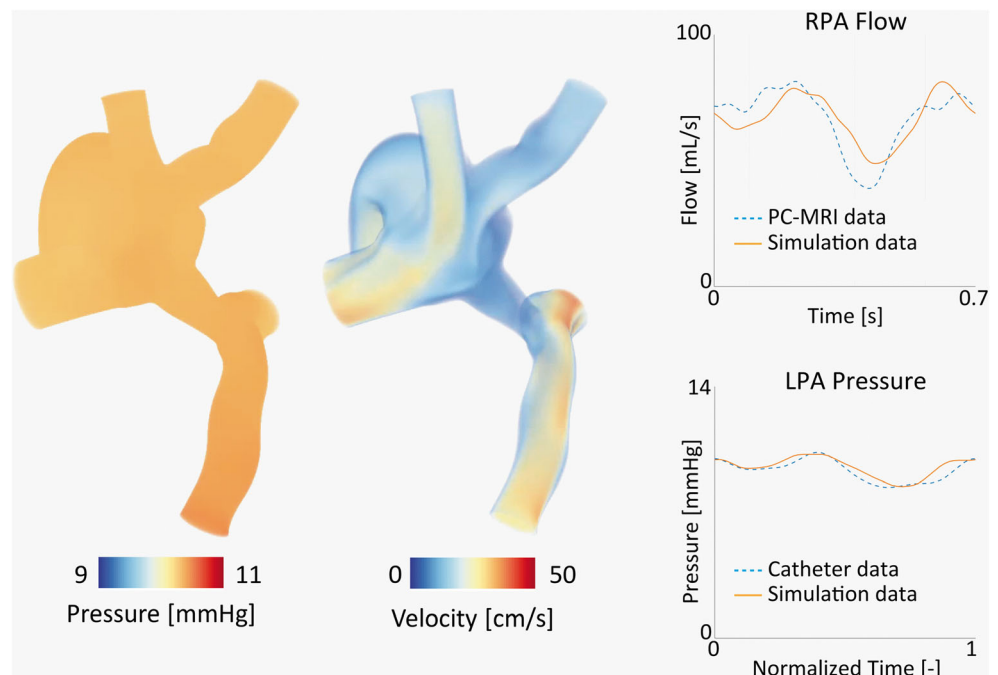
AZV azygos vein, FN Fontan conduit, LINV left innominate vein, LPA left pulmonary artery, MRI magnetic resonance imaging, RINV right innominate vein, RPA right pulmonary artery

on the values of the LPA and RPA Windkessel models were made until the difference in mean and pulse values relative to the data was less than 5%. A “particle tracking” postprocessing analysis was used to assess the distribution of HVF between both lungs [38]. A 1-mL bolus representing a control volume of HVF was injected in the FN and the RPA/LPA split of the particles defining the bolus was analyzed. All particles flowed into the LPA, leaving the RPA deprived from any HVF. This result is consistent with the presence of PAVMs in the right lung. Completion of this validated baseline solution achieves step 1 in Fig. 1.

Surgical Planning

Surgical revision of the FN was proposed to achieve a more balanced distribution of HVF between both lungs. Two options were considered, based on clinical feasibility. In option 1, Hepatic-to-Azygos, the FN is removed and an anastomosis is made from the HV to the AZV. In option 2, Fontan-to-Innominate, the FN is detached from the LPA and extended to the LINV. Figure 5 depicts the two proposed surgical options. Computations were performed to predict hemodynamics in both surgical options, leaving inflow and outflow conditions unchanged relative to the baseline solution, except for

Fig. 4 Step 1 of the surgical planning workflow: Left: Snapshot of pressure and velocity fields of the verified baseline solution. Here, boundary condition parameters were iteratively refined until a good match between computed and measured flow and pressure waveforms was achieved (right). LPA = left pulmonary artery, PC-MRI = phase-contrast magnetic resonance imaging, RPA = right pulmonary artery



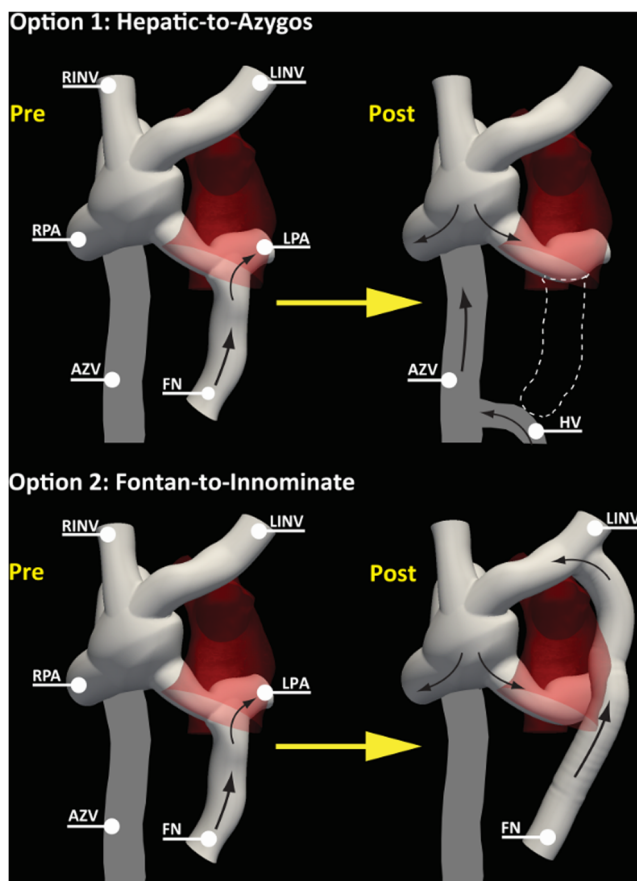


Fig. 5 Step 2 of the surgical planning workflow: Two surgical options were considered as potential repair solutions. Option 1 (Hepatic-to-Azygos) consists of the removal of the FN from the LPA and the anastomosis of the HV directly to the distal part of the AZV. Option 2 (Fontan-to-Innominate) consists of detaching the FN from the LPA and extending it to the LINV. The black arrows indicate the direction of the hepatic venous flow in each option. AZV = azygos vein, FN = Fontan conduit, HV = hepatic vein, LINV = innominate vein, LPA = left pulmonary artery, RPA = right pulmonary artery, RINV = right innominate vein

the inflow alterations resulting from the different surgical manipulations (step 2, Fig. 1). The RPA/LPA HVF distribution was calculated for each option using the bolus tracking techniques. Furthermore, to assess the sensitivity of HVF distribution to the time of bolus injection, the bolus tracking analysis was performed at 55 different time-points in the cardiac cycle.

Simulation Results of the Surgical Options

Computational results for both surgical options are summarized in Fig. 6. The Hepatic-to-Azygos option resulted in a mean RPA/LPA HVF distribution of 80:20 and a wide variability through the cardiac cycle in %HVF reaching the RPA (max. 88%, min. 62%). Conversely, the Fontan-to-Innominate option resulted in a mean RPA/LPA HVF distribution of 70:30 and a much smaller variability in %HVF reaching the RPA

(max. 77%, min. 63%). Due to the more balanced RPA/LPA HVF ratio and smaller variability over the cycle, the Fontan-to-Innominate option was selected after discussing it within the multidisciplinary research and surgical team.

Clinical Outcomes

The Fontan-to-Innominate surgical procedure was successfully performed. Figure 7 presents pre-operative and post-operative angiograms. The pre-operative angiogram shows a clear bias of HVF towards the left lung, in agreement with the particle tracking analysis of the baseline solution. Conversely, the post-operative angiogram showed a much more balanced distribution of HVF between the left and right lungs, consistent with our simulation results. At most recent clinical follow-up, 11 months post-operative, overall symptoms had improved. The patient denied shortness of breath and exercise intolerance. Furthermore, oxygen saturation at rest had increased from 82 to 96%, suggesting that increased levels of HVF reverted the progression of PAVMs.

Present and Future Challenges

Computational modeling techniques have the potential to aid cardiovascular disease research and clinical decision making [39]. Nonetheless, there are multiple obstacles in the way of routine clinical application.

Computations are time-consuming, typically requiring multiple days to run, despite advances in HPC processing speeds. Near real-time solutions are therefore not feasible and thus computations can only aid clinical decision making in elective cases.

The time-intensive and somewhat operator-dependent nature of model construction, parameterization, and validation also affects the clinical applicability of the workflow. Inconsistencies in clinical data can also potentially lead to inaccurate results [15]. Automated workflows relying on data-driven simulations, machine, and deep learning tools will help mitigate some of these issues. Ideally, surgical planning supported by computational modeling should involve clinicians and bioengineers working together in multidisciplinary teams. Clinicians should oversee informing the patient, acquiring necessary clinical data and proposing surgically feasible options. Engineers should then perform the analyses following the two-step workflow in Fig. 1 and extract clinically meaningful conclusions. Results should then be discussed in a multidisciplinary conference and subsequently presented to the patient.

Current modeling paradigms only predict acute hemodynamic responses immediately after the surgery. Short-

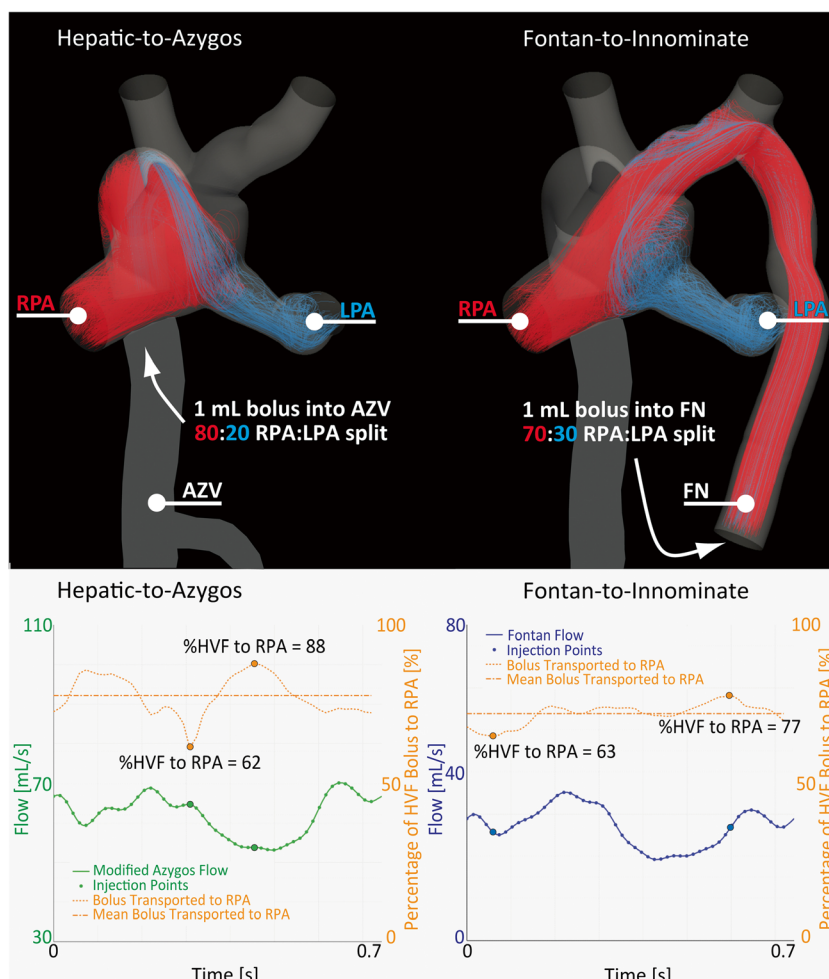


Fig. 6 HVF distribution for the two surgical options. Top panel: path lines of HVF distribution between RPA (red lines) and LPA (blue lines) for the Hepatic-to-Azygos and Fontan-to-Innominate options. The RPA/LPA HVF distribution is 80:20 and 70:30 in the Hepatic-to-Azygos and Fontan-to-Innominate options, respectively. Bottom panel: Analysis of percent of HVF transported to the RPA for 55 different bolus injection points. The injection points corresponding with maximum and minimum %HVF transported to the RPA are highlighted for each surgical scenario. The Hepatic-to-Azygos option shows a large variability in the %HVF

transported to the RPA (maximum and minimum values of 88 and 62%, respectively). In contrast, the Fontan-to-Innominate option shows a much smaller variability for the different bolus injection times (maximum and minimum values of 63 and 77%, respectively). These findings suggest that the Fontan-to-Innominate option is hemodynamically superior. AZV = azygos vein, FN = Fontan conduit, HVF = hepatic venous flow, LPA = left pulmonary artery, RPA = right pulmonary artery, T = time



Fig. 7 Angiographic imaging was used to visualize the transport of HVF to the lungs. Left: pre-operative angiogram shows that contrast injected in the FN is being transported exclusively to the LPA. The right lung is completely deprived from HVF. Right: post-operative angiogram reveals

that contrast injected in the FN now reaches both lungs, with arguably larger presence of contrast in the right lung. These findings agree well with our computational results. FN = Fontan conduit, HVF = hepatic venous flow

term hemodynamic adaptations (intrinsic or extrinsic) are usually left out of the simulation pipeline. Progress has been recently made in developing computational methods to predict short-term hemodynamic extrinsic (e.g., baroreflex effects [40]) or intrinsic adaptations (e.g., metabolic and adrenergic responses in the coronary bed [41]). A bigger challenge is to predict the long-term response of the surgical solution due to tissue growth-and-remodeling. Although theoretical foundations for stress-mediated vascular growth and remodeling are currently being explored [42], these are far from ready to be applied in clinical decision making.

In the future, guidelines should be created to support best practices resulting in reproducible computational approaches for specific surgical procedures. The outcomes of the computer-guided surgical planning could then be added to the diagnostic workup. Additionally, training courses in computational modeling geared towards surgical planning can be held to train participants in producing reliable simulation workflows.

Conclusions

The potential applications for computational modeling in the cardiovascular field are numerous. Patient-specific simulations enable prediction of hemodynamic outcomes in different interventional procedures, allowing development of individually tailored treatment plans in complex vascular pathologies. In order for these analyses to be routinely used in clinical practice, the accuracy of the simulation results needs to be assessed. Multidisciplinary collaboration between biomedical engineers and clinicians is key to provide accurate computational simulations that benefit research and treatment of cardiovascular disease.

Acknowledgements The authors gratefully acknowledge financial support from the European Research Council under the European Union's Seventh Framework Programme (FP/2007-2013)/ERC Grant Agreement No. 307532, the Edward B. Diethrich Professorship, the Bob and Ann Aikens Aortic Grants Program, and the Frankel Cardiovascular Center. Computing resources were provided by the National Science Foundation via grant 1531752 MRI: Acquisition of Conflux, A Novel Platform for Data-Driven Computational Physics (Tech. Monitor: Ed Walker).

Compliance with Ethical Standards

Conflict of interest The authors declare that they have no conflict of interest related to the contents of the manuscript.

Ethics Approval and Consent to Participate All procedures followed were in accordance with the ethical standards of the institutional review board (University of Michigan record number HUM00136247) and with the Helsinki Declaration of 1975 and its later amendments. The need for patient consent for the preparation of this manuscript was waived.

References

- Cecchi, E., Giglioli, C., Valente, S., Lazzeri, C., Gensini, G. F., Abbate, R., et al. (2011). Role of hemodynamic shear stress in cardiovascular disease. *Atherosclerosis*, *214*, 249–256. <https://doi.org/10.1016/j.atherosclerosis.2010.09.008>.
- Taylor, C. A., & Figueroa, C. A. (2009). Patient-specific modeling of cardiovascular mechanics. *Annual Review of Biomedical Engineering*, *11*, 109–134. <https://doi.org/10.1146/annurev.bioeng.10.061807.160521>.
- Cuomo, F., Rocchianca, S., Dillon-Murphy, D., Xiao, N., Humphrey, J. D., & Figueroa, C. A. (2017). Effects of age-associated regional changes in aortic stiffness on human hemodynamics revealed by computational modeling. *PLoS One*, *12*. <https://doi.org/10.1371/journal.pone.0173177>.
- Taylor, C. A., Fonte, T. A., & Min, J. K. (2013). Computational fluid dynamics applied to cardiac computed tomography for noninvasive quantification of fractional flow reserve. *Journal of the American College of Cardiology*, *61*, 2233–2241. <https://doi.org/10.1016/j.jacc.2012.11.083>.
- Figueroa, C. A., Yeh, V., Taylor, C. A., Gorrepati, M. L., & Zarins, C. K. (2010). In vivo displacement force (DF) is higher in patients who experience aortic endograft migration: a 3D computational analysis. *Journal of Vascular Surgery*, *51*, 93S.
- Trusty, P. M., Wei, Z., Tree, M., Kanter, K. R., Fogel, M. A., Yoganathan, A. P., et al. (2017). Local hemodynamic differences between commercially available Y-Grafts and traditional fontan baffles under simulated exercise conditions: implications for exercise tolerance. *Cardiovascular Engineering and Technology*, *8*, 390–399. <https://doi.org/10.1007/s13239-017-0310-5>.
- Nauta, F. J., Lau, K. D., Arthurs, C. J., Eagle, K. A., Williams, D. M., Trimarchi, S., et al. (2017). Computational fluid dynamics and aortic thrombus formation following thoracic endovascular aortic repair. *The Annals of Thoracic Surgery*. <https://doi.org/10.1016/j.athoracsur.2016.09.067>.
- Tang, E., Wei, Z., Whitehead, K. K., Khiabani, R. H., Restrepo, M., Mirabella, L., et al. (2017). Effect of Fontan geometry on exercise haemodynamics and its potential implications. *Heart*, *103*, 1806–1812. <https://doi.org/10.1136/heartjnl-2016-310855>.
- Antiga L, Steinman DA. (2008). The vascular modeling toolkit. <http://www.vmtk.org>.
- Materialise Mimics n.d. <http://biomedical.materialise.com/mimics>.
- CRIMSON. The software for Cardiovascular Modelling and Simulation n.d. <http://www.crimson.software>.
- Vieira, M. S., Hussain, T., & Figueroa, C. A. (2015). Patient-specific image-based computational modeling in congenital heart disease: a clinician perspective. *J Cardiol Ther*, *2*, 436–448.
- Sahni, O., Müller, J., Jansen, K. E., Shephard, M. S., & Taylor, C. A. (2006). Efficient anisotropic adaptive discretization of the cardiovascular system. *Computer Methods in Applied Mechanics and Engineering*, *195*, 5634–5655. <https://doi.org/10.1016/j.cma.2005.10.018>.
- Vignon-Clementel, I. E., Figueroa, C. A., Jansen, K. E., & Taylor, C. A. (2010). Outflow boundary conditions for 3D simulations of non-periodic blood flow and pressure fields in deformable arteries. *Computer Methods in Biomechanics and Biomedical Engineering*, *13*, 625–640. <https://doi.org/10.1080/10255840903413565>.
- Alastruey, J., Xiao, N., Fok, H., Schaeffter, T., & Figueroa, C. A. (2016). On the impact of modelling assumptions in multi-scale, subject-specific models of aortic haemodynamics. *J R Soc Interface*, *13*. <https://doi.org/10.1098/rsif.2016.0073>.
- Pelc, N. J., Sommer, F. G., Li, K. C., Brosnan, T. J., Herfkens, R. J., Enzmann, D. R., et al. (1994). Quantitative magnetic resonance flow imaging. *Magnetic Resonance Quarterly*, *10*(3), 125–147.

17. Bushberg, J. T., Seibert, J. A., Leidholdt, E. M., & Boone, J. M. (2012). *The essential physics of medical imaging* (Third ed.). Philadelphia: Lippincott Williams & Wilkins.
18. Hoskins, P., Martin, K., & Thrush, A. (2010). *Diagnostic ultrasound: physics and equipment* (2nd ed.). Cambridge: Cambridge University Press. <https://doi.org/10.2967/jnumed.112.105395>.
19. Gatehouse, P. D., Keegan, J., Crowe, L. A., Masood, S., Mohiaddin, R. H., Kreitner, K.-F., et al. (2005). Applications of phase-contrast flow and velocity imaging in cardiovascular MRI. *European Radiology*, *15*, 2172–2184. <https://doi.org/10.1007/s00330-005-2829-3>.
20. de Beaufort, H. W. L., Nauta, F. J. H., Conti, M., Cellitti, E., Trentin, C., Faggiano, E., et al. (2017). Extensibility and distensibility of the thoracic aorta in patients with aneurysm. *European Journal of Vascular and Endovascular Surgery*, *53*, 199–205. <https://doi.org/10.1016/j.ejvs.2016.11.018>.
21. Cuomo, F., Ferruzzi, J., Humphrey, J. D., & Figueroa, C. A. (2015). An experimental–computational study of catheter induced alterations in pulse wave velocity in anesthetized mice. *Annals of Biomedical Engineering*, *43*, 1555–1570. <https://doi.org/10.1007/s10439-015-1272-0>.
22. Fagard, R., & Conway, J. (1990). Measurement of cardiac output: Fick principle using catheterization. *European Heart Journal*, *11*, 1–5. https://doi.org/10.1093/eurheartj/11.suppl_1.1.
23. Pugsley, J., & Lerner, A. B. (2010). Cardiac output monitoring: is there a gold standard and how do the newer technologies compare? *Seminars in Cardiothoracic and Vascular Anesthesia*, *14*, 274–282. <https://doi.org/10.1177/1089253210386386>.
24. Figueroa, C. A., Vignon-Clementel, I. E., Jansen, K. E., Hughes, T. J. R., & Taylor, C. A. (2006). A coupled momentum method for modeling blood flow in three-dimensional deformable arteries. *Computer Methods in Applied Mechanics and Engineering*, *195*, 5685–5706. <https://doi.org/10.1016/j.cma.2005.11.011>.
25. Brown, A. G., Shi, Y., Marzo, A., Staicu, C., Valverde, I., Beerbaum, P., et al. (2012). Accuracy vs. computational time: translating aortic simulations to the clinic. *Journal of Biomechanics*, *45*, 516–523. <https://doi.org/10.1016/j.jbiomech.2011.11.041>.
26. Prasad, A., To, L. K., Gorrepati, M. L., Zarins, C. K., & Figueroa, C. A. (2011). Computational analysis of stresses acting on intermodular junctions in thoracic aortic endografts. *Journal of Endovascular Therapy*, *18*, 559–568. <https://doi.org/10.1583/11-3472.1>.
27. Les, A. S., Shadden, S. C., Figueroa, C. A., Park, J. M., Tedesco, M. M., Herfkens, R. J., et al. (2010). Quantification of hemodynamics in abdominal aortic aneurysms during rest and exercise using magnetic resonance imaging and computational fluid dynamics. *Annals of Biomedical Engineering*, *38*, 1288–1313. <https://doi.org/10.1007/s10439-010-9949-x>.
28. Fontan, F., & Baudet, E. (1971). Surgical repair of tricuspid atresia. *Thorax*, *26*, 240–248.
29. Gewillig, M. (2005). The Fontan circulation. *Heart*, *91*, 839–846. <https://doi.org/10.1136/hrt.2004.051789>.
30. Duncan, B. W., & Desai, S. (2003). Pulmonary arteriovenous malformations after cavopulmonary anastomosis. *The Annals of Thoracic Surgery*, *76*, 1759–1766.
31. Srivastava, D., Preminger, T., Lock, J. E., Mandell, V., Keane, J. F., Mayer, J. E., et al. (1995). Hepatic venous blood and the development of pulmonary arteriovenous malformations in congenital heart disease. *Circulation*, *92*, 1217–1222.
32. Pike, N. A., Vricella, L. A., Feinstein, J. A., Black, M. D., & Reitz, B. A. (2004). Regression of severe pulmonary arteriovenous malformations after Fontan revision and “hepatic factor” rerouting. *The Annals of Thoracic Surgery*, *78*, 697–699. <https://doi.org/10.1016/j.athoracsur.2004.02.003>.
33. McElhinney, D. B., Marx, G. R., Marshall, A. C., Mayer, J. E., & Del Nido, P. J. (2011). Cavopulmonary pathway modification in patients with heterotaxy and newly diagnosed or persistent pulmonary arteriovenous malformations after a modified Fontan operation. *The Journal of Thoracic and Cardiovascular Surgery*, *141*, 1362–70.e1. <https://doi.org/10.1016/j.jtcvs.2010.08.088>.
34. Shah, M. J., Rychik, J., Fogel, M. A., Murphy, J. D., & Jacobs, M. L. (1997). Pulmonary AV malformations after superior cavopulmonary connection: resolution after inclusion of hepatic veins in the pulmonary circulation. *The Annals of Thoracic Surgery*, *63*, 960–963.
35. de Zélicourt, D. A., Haggerty, C. M., Sundaeswaran, K. S., Whited, B. S., Rossignac, J. R., Kanter, K. R., et al. (2011). Individualized computer-based surgical planning to address pulmonary arteriovenous malformations in patients with a single ventricle with an interrupted inferior vena cava and azygous continuation. *The Journal of Thoracic and Cardiovascular Surgery*, *141*, 1170–1177. <https://doi.org/10.1016/j.jtcvs.2010.11.032>.
36. Kawashima, Y., Kitamura, S., Matsuda, H., Shimazaki, Y., Nakano, S., & Hirose, H. (1984). Total cavopulmonary shunt operation in complex cardiac anomalies. A new operation. *The Journal of Thoracic and Cardiovascular Surgery*, *87*, 74–81.
37. Helps, E. P. W., & McDonald, D. A. (1954). Observations on laminar flow in veins. *The Journal of Physiology*, *124*, 631–639. <https://doi.org/10.1113/jphysiol.1954.sp005135>.
38. Shadden, S. C., & Hendabadi, S. (2013). Potential fluid mechanic pathways of platelet activation. *Biomechanics and Modeling in Mechanobiology*, *12*, 467–474. <https://doi.org/10.1007/s10237-012-0417-4>.
39. Biglino G, Capelli C, Bruse J, Bosi GM, Taylor AM, Schievano S. (2016). Computational modelling for congenital heart disease: how far are we from clinical translation? *Heart*, 1–6. doi:<https://doi.org/10.1136/heartjnl-2016-310423>.
40. Lau, K. D., & Figueroa, C. A. (2015). Simulation of short-term pressure regulation during the tilt test in a coupled 3D-0D closed-loop model of the circulation. *Biomechanics and Modeling in Mechanobiology*, *14*, 915–929. <https://doi.org/10.1007/s10237-014-0645-x>.
41. Arthurs, C. J., Lau, K. D., Asress, K. N., Redwood, S. R., & Figueroa, C. A. (2016). A mathematical model of coronary blood flow control: simulation of patient-specific three-dimensional hemodynamics during exercise. *Am J Physiol - Hear Circ Physiol*, *310*, H1242–H1258. <https://doi.org/10.1152/ajpheart.00517.2015>.
42. Figueroa, C. A., Baek, S., Taylor, C. A., & Humphrey, J. D. (2009). A computational framework for fluid-solid-growth modeling in cardiovascular simulations. *Computer Methods in Applied Mechanics and Engineering*, *198*, 3583–3602. <https://doi.org/10.1016/j.cma.2008.09.013>.